Calcif Tissue Int (2008) 82:66–76
DOI 10.1007/s00223-007-9098-x

Phenotypic Characteristics of Bone in Carbonic Anhydrase II-Deficient Mice

David S. Margolis · John A. Szivek · Li-Wen Lai · Yeong-Hau H. Lien

Received: 20 June 2007 / Accepted: 4 December 2007 / Published online: 4 January 2008

Abstract Carbonic anhydrase II (CAII)-deficient mice were created to study the syndrome of CAII deficiency in humans including osteopetrosis, renal tubular acidosis, and cerebral calcification. Although CAII mice have renal tubular acidosis, studies that analyzed only cortical bones found no changes characteristic of osteopetrosis. Consistent with previous studies, the tibiae of CAII-deficient mice were significantly smaller than those of wild-type (WT) mice (28.7 ± 0.9 vs. 43.6 ± 3.7 mg; $p < 0.005$), and the normalized cortical bone volume of CAII-deficient mice ($79.3 \pm 2.2\%$) was within 5% of that of WT mice ($82.7 \pm 2.3\%$; $p < 0.05$), however, metaphyseal widening of the tibial plateau was noted in CAII-deficient mice, consistent with osteopetrosis. In contrast to cortical bone, trabecular bone volume demonstrated a nearly 50% increase in CAII-deficient mice ($22.9 \pm 3.5\%$ in CAII, compared to $15.3 \pm 1.6\%$ in WT; $p < 0.001$). In addition, histomorphometry demonstrated that bone formation rate was decreased by 68% in cortical bone (4.77 ± 1.65 $\mu m^3/\mu m^2$/day in WT vs. 2.07 ± 1.71 $\mu m^3/\mu m^2$/day in CAII mice; $p < 0.05$) and 55% in trabecular bone (0.617 ± 0.230 $\mu m^3/\mu m^2$/day in WT vs. 0.272 ± 0.114 $\mu m^3/\mu m^2$/day in CAII mice; $p < 0.05$) in CAII-deficient mice. The number of osteoclasts was significantly increased (67%) in CAII-deficient mice, while osteoblast number was not different from that in WT mice. The metaphyseal widening and changes in the trabecular bone are consistent with osteopetrosis, making the CAII-deficient mouse a valuable model of human disease.

Keywords Carbonic anhydrase II · Osteopetrosis · Renal tubular acidosis · Osteoclast · Osteoblast

D. S. Margolis · J. A. Szivek
Orthopaedic Research Lab, Department of Orthopaedic Surgery, University of Arizona, Tucson, AZ 85721, USA
e-mail: dsm@u.arizona.edu

L.-W. Lai · Y.-H. H. Lien (✉)
Department of Medicine, University of Arizona, 1501 North Campbell Avenue, Room 6413, Tucson, AZ 85724, USA
e-mail: lien@email.arizona.edu

Bone tissue is dynamic due to the bone resorptive activity of osteoclasts and the bone forming activity of osteoblasts, both of which are required to maintain optimal bone mass. An imbalance between the activity of osteoclasts and that of osteoblasts can lead to disease states including osteopetrosis and osteoporosis. Osteopetrosis is a group of inheritable diseases that result in increased bone density due to osteoclast defects [1].

The first genetic mutation discovered that was responsible for osteopetrosis was a carbonic anhydrase II (CAII) deficiency, which also causes renal tubular acidosis and cerebral calcification [2–4]. In order to study the features of CAII deficiency, a mouse model was created using chemically induced mutagenesis [5]. This mouse model of CAII deficiency demonstrated many of the pathological features of human disease, including stunted growth and renal tubular acidosis; however, a notable feature of the CAII-deficient mouse was that it lacked the osteopetrosis and cerebral calcifications that are seen in patients with this defect [5]. CAII-deficient mice displayed smaller bones compared to wild-type (WT) mice, because the mice have a lower body weight [5], but even aged CAII-deficient mice did not develop severe osteopetrosis, as was apparent by the visibility of the marrow cavities on planar x-rays and the normal/low radiopacity of the bones [5]. To date only one quantitative study has been performed to confirm this

observation. In that study it was noted that the cortical bone in CAII-deficient mice had a similar bending modulus and brittleness compared to WT mice [6]. Furthermore, the study reported no differences in the histological structure of cortical bone in CAII-deficient mice, although the parameters that were measured were not discussed beyond confirming the presence of marrow cavities in the long bones [6]. No quantitative study has ever been performed on the trabecular bone in CAII-deficient mice.

While it is clear that CAII-deficient mice do not have a phenotype of severe osteopetrosis, the skeletal disease in patients with CAII deficiency is variable and less severe than the malignant forms of osteopetrosis [1]. Indeed, one report of a patient with CAII deficiency did not demonstrate radiographic changes sufficient to diagnose osteopetrosis [4]. The clinical heterogeneity of osteopetrosis in CAII-deficient patients warranted a more in-depth look into the bone structure of CAII-deficient mice, particularly if the mice display a skeletal phenotype. In this present study, we performed histology, histomorphometry, and high-resolution μCT analyses to characterize both trabecular and cortical bone in the tibiae of CAII-deficient mice to determine whether the mice display any characteristics consistent with osteopetrosis.

Materials and Methods

Animals

National Institutes of Health guidelines for the care and use of laboratory animals (NIH publication no. 82–23, rev. 1985) and the Guideline Principles in the Care and Use of Animals (Council of the American Physiological Society, 1991) were followed during this study. The C3H strain of CAII-deficient mice was developed from the original C57BL/6J CAR-2 mice [5] as described previously [7, 8]. The mice were backcrossed to C3H mice for more than five generations and are considered congenic to these mice. They are maintained as a homozygous CAII-deficient colony. The resulting homozygous deficient mice have similar growth curves and urine pH [7, 8] compared to the original mutant mouse [5] and carry a nonsense mutation resulting in early termination of translation of the CAII gene (Gln155/term) [9]. These CAII-deficient mice have mixed metabolic and respiratory acidosis, with a low arterial blood pH, in the range of 7.18–7.25 [7]. Normal C3H mice were used as controls in this experiment. The six male C3H mice and six male CAII-deficient mice were 90 days old at the time of sacrifice. At both 13 and 3 days prior to sacrifice, the mice were labeled with calcein (Sigma,
St. Louis, MO) subcutaneously at a dose of 15 mg/kg. Following sacrifice, the right tibiae were explanted, cleaned of soft tissue, and placed in a 70% ethanol solution in preparation for histology and histomorphometry.

Gross analysis of tibiae

Gross measurements were performed on the left tibia prior to freezing the tibiae at –20°C until μCT imaging. Measurements were collected using calipers with a 0.05-mm resolution. The width of the tibial plateaus was measured from the medial to the lateral condyles. The width of the ankle was measured from the medial to the lateral malleoli, and the length of the tibiae was measured from the medial condyle to the medial malleolus.

Histology and histomorphometry

Following sacrifice, the tibiae of the calcein-labeled mice were immediately dehydrated in a series of ethanol solutions and then embedded in polymethylmethacrylate using a previously reported technique [10]. One cross section was cut perpendicular to the long axis of the bone, through the tibia-fibular junction, and another midsagittal section was cut through the tibial plateau. The cross sections were ground to a thickness of $\sim$10 μm and polished with 0.5 μm alumina using a Leco GP-25 Grinder/Polisher (Leco Corp., St. Joseph, MI). The ground and polished sections were stained using mineralized bone stain (MIBS) following a published procedure [11]. Images of the bones were collected using an Optronics digital imaging system consisting of an Olympus camera and Magnafire software (Optronics, Goleta, CA) coupled to a Machintosh G3 computer. Image analysis was performed using Image J software for the Machintosh OS X operating system, developed by the National Institutes of Health (Research Services Branch, NIMH). Cortical bone was analyzed at the tibia-fibula junction, and the trabecular bone was analyzed in the tibial plateau in a region extending 0.9 mm distal to the epiphyseal plate. The quantitative histological measurements included the following parameters: bone, marrow cavity, and osteiod areas (mm^2), as well as endosteal and periosteal perimeters (mm). The tissue area was calculated as the sum of the bone, marrow, and osteoid areas. The bone volume (BV/TV; %) was calculated as the bone area divided by the tissue area, multiplied by 100 to convert it to a percentage. Marrow cavity volume (MaV/TV; %) and osteoid volume (OS/TV; %) were calculated the same way.

The quantitative histomorphometry parameters measured under fluorescent light included the single-label length, double-label length, and interlabel distance. In cortical bone the histomorphometry parameters were calculated

separately for the endosteal and periosteal surfaces. The mineral apposition rate (MAR; μm/day) was calculated as the distance between the calcein double labels divided by the days between administration of calcein. The mineralizing surface (MS) was calculated as the sum of the length of the double labels plus one-half the length of the single labels. The labeled surface (%) was calculated as the MS divided by the bone perimeter and multiplied by 100%. The bone formation rate, BFR/BS ($\mu m^3/\mu m^2$/day), was calculated as the product of MAR and MS, divided by the perimeter. In the trabecular bone of the tibial plateau the bone formation rate was also calculated using a bone volume referent, BFR/BV (%/day), which was calculated as the product of MAR and MS, divided by the cortical bone area and multiplied by 100%. All histomorphometry parameters were determined using the guidelines set forth by the American Society of Bone and Mineral Research [12].

For quantification of osteoclasts and osteoblasts, and transmission electron microscopy study, the bones of an additional three C3H and three CAII-deficient mice were isolated following perfusion with 10% formalin and post-fixation in either 10% formalin for 24 h in preparation for histology or in half-strength Karnovsky's fixative (2.5% glutaraldehyde and 2% paraformaldehyde in 0.1 M cacodylate buffer) for 24 h in preparation for transmission electron microscopy.

Formalin-fixed tibiae were decalcified in rapid decalcifier (Apex Engineering Products Co, Aurora, IL) for 3 h, embedded in paraffin, and cut into 3-μm-thick midsagittal sections using a Microm HM 355 S microtome (Mikron Instruments Inc., San Marcos, CA). The sections were stained for tartrate-resistant acid phosphatase (TRAP) using a histochemical kit (Sigma, St. Louis, MO) to identify osteoclasts and with hematoxylin and eosin to count osteoblasts. Osteoclast number (no./mm) was calculated as the number of multinucleated (two or or more nuclei) TRAP-positive cells per millimeter of bone surface. Osteoclast surface (Oc S/BS; %) was calculated as the ratio of cell surface to bone surface multiplied by 100%. Osteoblast number and surface were calculated similarly.

Transmission electron microscopy

The tibiae fixed in half-strength Karnovsky's fixative for 24 h were decalcified using Formical-2000 (Decal Chemical Corp., Tallman, NY) for 3 h. The bones were washed, postfixed with 2% OsO_4, dehydrated, and embedded in Spurr's resin [13]. One-micrometer-thick sections were cut on a Leica UCT ultramicrotome (Leica Microsystems Inc., Bannockburn, IL) and were imaged on a CM12 transmission electron microscope (FEI Co., Hillsboro, OR). Osteoclasts were identified as multinucleated cells that were attached to bone.

μCT imaging

A Scanco Medical μCT 20 (Scanco, Switzerland) was used to scan the tibias as previously described [14]. The trabecular bone in the tibial plateau, extending 0.9 mm below the epiphyseal plate, was analyzed. In addition to the trabecular bone, the cortical bone was analyzed at the tibia-fibular junction in the same place that histomorphometry was performed on the contralateral tibia. The resolution of the scans was 9 μm. The trabecular bone was analyzed for bone volume (BV/TV; %), trabecular number (mm^{-1}), trabecular thickness (mm), trabecular spacing (mm), and ratio of bone surface to bone volume (BS/BV; mm^{-1}). The cortical bone was analyzed for nonnormalized cortical bone volume (mm^3), normalized bone volume (BV/TV; %), cortical bone thickness (mm), and ratio of bone surface to bone volume (BS/BV; mm^{-1}).

Bone mineral content analysis

A second set of μCT images was collected at a resolution of 9 μm, which included a set of phantoms ranging in density from 0 to 1000 mg of hydroxyapatite/ml (Gammasonics, Australia) placed in the sample holder with the bone. Ten cross-sectional images taken through the tibial plateau and 10 cross-sectional images taken through the tibia-fibula junction were analyzed for each mouse. The cross-sectional images were imported into Image J software for the Macintosh OS X operating system (Research Services Branch, NIMH). In each image the mean gray value was measured from the phantoms and used to generate a standard curve relating the mean gray value to the mineral density using a linear curve. The bone area in each cross-sectional image bone was selected using a threshold analysis with a lower limit of 60 and an upper limit of 500. These values were chosen as they gave similar bone volumes to those found using the software developed by Scanco for the μCT analysis as well as the values measured using histology. The standard curve generated in each slice was used to convert mean the gray value measured for bone into a bone mineral density.

Statistical analysis

Kurtosis was noted in some of the histological measurements, so determination of statistical significance for all data was carried out using a Mann-Whitney U test, with $p < 0.05$ considered significant.

Table 1 Gross analysis of tibiae[a]

	Wild-type mice	CAII-deficient mice	% change	*p*
Dry bone mass (mg)	43.6 ± 3.7	28.7 ± 0.9	↓ 34.2	<0.005
Width of tibial plateau (mm)	2.88 ± 0.20	2.77 ± 0.06	↓ 3.8	NS
Width of ankle (mm)	2.52 ± 0.13	2.04 ± 0.09	↓ 19.0	<0.005
Length of tibia (mm)	17.83 ± 0.37	16.51 ± 0.16	↓ 7.4	<0.005

[a] Data expressed as mean ± standard deviation

Results

Gross analysis of tibiae

The weight of the tibiae of CAII-deficient mice was 34% lower than that of WT mice (Table 1). The tibiae were shorter and had a decreased width at the ankle compared to WT mice. The width of the tibial plateau was the same in CAII-deficient and WT mice (Table 1).

Histology

The smaller size of the tibiae of the CAII-deficient mice was demonstrated by the 32.3% lower cross-sectional cortical bone areas and 14.7% smaller periosteal perimeters of the tibia-fibula junction (Figs. 1A and B, Table 2). When normalized to the tissue volume, the CAII-deficient mice showed a small (4%), but statistically significant decrease in bone volume (Table 2). The number of osteoclasts was increased by 67% and the osteoclast surface was increased by 122% in CAII-deficient mice (Fig. 3, Table 2). Osteoclasts in CAII-deficient mice appeared to resorb bone, as many formed lacunae with scalloped edges. Osteoblast number and osteoblast surface were normal in CAII-deficient mice (Table 2).

Transmission electron microscopy

Osteoclasts in CAII-deficient mice look similar to those in WT mice. The cells of both WT and CAII-deficient osteoclasts have abundant mitochondria and ruffled borders (Fig. 3).

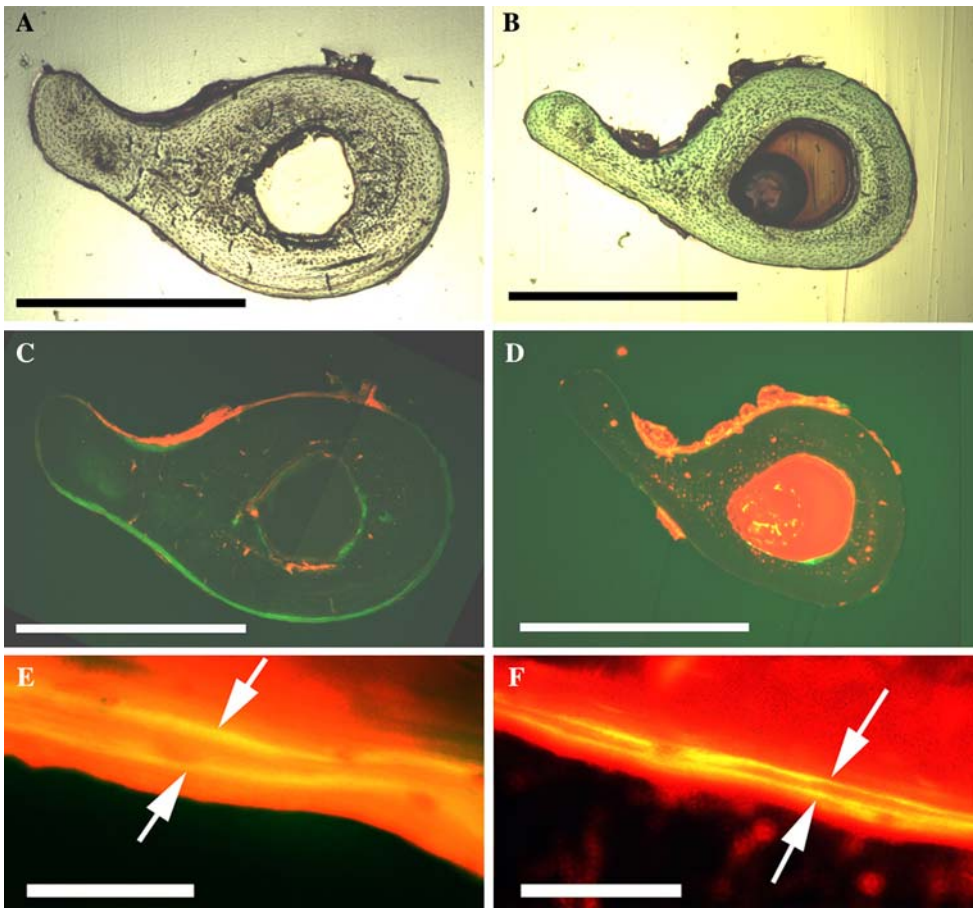

Fig. 1 Cross sections through the tibia-fibula junction of WT (left) and CAII-deficient (right) mice. CAII-deficient mice (**B**) have smaller bones with a similar bone volume and an increased marrow cavity volume compared to WT mice (**A**). Histomorphometry demonstrated a decrease in the length of calcein-labeled surface (**C**, **D**). In addition, the mineral apposition rate was lower in CAII-deficient mice, as indicated by the decreased distance between the caclein labels (**E**, **F**; arrows). Scale bar = 1 mm (A–D) and 50 μm in (E, F)

Table 2 Histology and histomorphometry[a]

	Wild-type mice	CAII-deficient mice	% change	*p*
Cortical bone				
Cross-sectional area (mm^2)	0.967 ± 0.043	0.655 ± 0.041	↓ 32.3%	<0.001
BV/TV (%)	82.7 ± 2.3	79.3 ± 2.2	↓ 4.1%	<0.05
MaV/TV (%)	16.2 ± 2.0	20.5 ± 2.3	↑ 26.5%	<0.05
OsV/TV (5%)	1.1 ± 0.5	0.3 ± 0.4	↓ 72.7%	<0.05
Periosteal				
Perimeter (mm)	5.043 ± 0.156	4.304 ± 0.255	↓ 14.7%	<0.001
Labeled surface (%)	59.2 ± 11.5	33.9 ± 16.8	↓ 42.7%	<0.01
Mineral apposition rate (μm/day)	1.296 ± 0.455	0.582 ± 0.468	↓ 55.1%	<0.01
BFR/BS ($\mu m^3/\mu m^2$/day)	0.795 ± 0.373	0.254 ± 0.270	↓ 68.1%	<0.01
Endosteal				
Perimeter (mm)	1.750 ± 0.118	1.645 ± 0.235	↓ 6.0%	NS
Labeled surface (%)	30.5 ± 20.2	7.4 ± 5.3	↓ 75.7%	<0.05
Mineral apposition rate (μm/day)	0.811 ± 0.380	—[b]	—	—
BFR/BS ($\mu m^3/\mu m^2$/day)	0.288 ± 0.223	—	—	—
Trabecular bone				
BV/TV (%)	15.3 ± 1.6	22.9 ± 3.5	↑ 49.7%	<0.001
MaV/TV (%)	82.4 ± 2.9	75.1 ± 3.2	↓ 8.9%	<0.001
OsV/TV (5%)	2.3 ± 2.0	2.0 ± 0.8	↓ 13.0%	NS
Labeled surface (%)	33.7 ± 5.4	22.0 ± 4.9	↓ 34.7%	<0.005
Mineral apposition rate (μm/day)	1.809 ± 0.564	1.196 ± 0.310	↓ 33.9%	NS
BFR/BS ($\mu m^3/\mu m^2$/day)	0.617 ± 0.230	0.272 ± 0.114	↓ 55.9%	<0.005
BFR/BV (%/day)	2.72 ± 0.99	1.35 ± 0.64	↓ 50.4%	<0.01
No. osteoblasts/mm	14.5 ± 1.0	15.9 ± 0.3	↑ 9.4%	NS
Osteoblast surface (%)	23.0 ± 2.7	19.0 ± 3.6	↓ 17.2%	NS
No. osteoclasts/mm	2.7 ± 0.6	4.5 ± 0.7	↑ 67.1%	<0.05
Osteoclast surface (%)	9.3 ± 3.5	20.7 ± 4.5	↑ 122.4%	<0.05

Note. Cortical bone parameters were measured from the tibia-fibula junction. Trabecular bone parameters were measured from the tibial plateau

[a] Data expressed as mean ± standard deviation

[b] A measurement was not taken because there was not a double label on the endosteal surface

Histomorphometry

At the tibia-fibula junction the periosteal bone formation rate (BFR/BS) was 68% lower in CAII-deficient mice, and this difference was due to a decrease in both the mineral apposition rate and the amount of labeled surface (Figs. 1 C–F, Table 2). Endosteal mineral apposition rate and bone formation rate were not reported at the tibia-fibula junction because only one CAII deficient mouse had a calcein double label present on the endosteal surface (Table 2). However, in the CAII-deficient mouse with an endosteal calcein double label, the MAR was 0.660 μm/day (18% decrease compared to the average endosteal MAR of WT mice; Table 2), and the BFR/BS was 0.109 $\mu m^3/\mu m^2$/day (62% decrease).

The trabecular bone of the tibial plateau showed a nearly 50% increase in bone volume compared to that of WT mice (Table 2). The trabeculae in both WT and CAII-deficient mice appeared normal and were aligned along the long axis of the bone; however, the number of trabeculae was increased in CAII-deficient mice and they were spaced closer together (Fig. 2). Similar to what was seen in the cortical bone, the bone formation rates were decreased by more than 50% in the trabecular bone (Table 2). While both the amount of labeled surface and the mineral apposition rate were decreased approximately 30% in the trabecular bone, this difference was only statistically significant for the decreased labeled surface (Table 2).

μCT imaging

μCT analysis of cortical bone at the tibia-fibular junction gave similar results to the histological analysis, demonstrating a 43% decrease in absolute cortical bone volume but only a 5% decrease in normalized bone volume (Table 3). In addition, CAII-deficient mice had a thinner cortical bone and a higher surface-to-bone volume ratio (Table 3).

μCT analysis of trabecular bone in the tibial plateau (Table 3) gave similar results compared to the histological analysis (Table 2), and it was noted that the increase

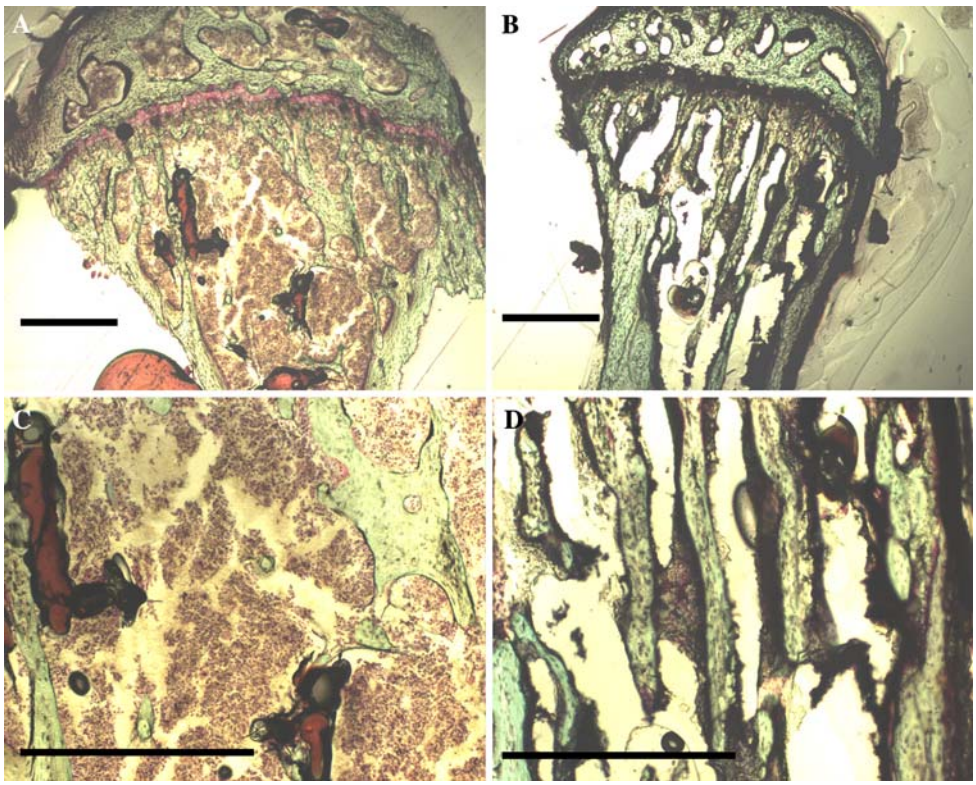

Fig. 2 Sagittal cross sections through the tibial plateau of WT (left) and CAII-deficient (right) mice. Low (**A**, **B**)- and high (**C**, **D**)-magnification images demonstrate that CAII-deficient mice have increased trabecular bone volume due to an increased number of trabeculae. The trabecular bone of CAII-deficient mice appears to be thinner and spaced closer together than the trabeculae of WT mice. Scale bar = 1 mm

in bone volume was due to an increased number of trabecula that were spaced closer together (Fig. 4), as the trabecular thickness was decreased in CAII-deficient mice (Table 3).

Bone mineral content analysis

The bone mineral content was lower in the cortical and trabecular bone of CAII-deficient mice (Table 3). While statistically significant in both locations, there was a <5% decrease in the cortical bone density and a >10% decrease in the trabecular bone density (Table 3).

Discussion

Although CAII-deficient mice and patients have similar pathological changes in blood pH and growth curves, CAII-deficient mice were not previously considered a good model of human disease because the mice did not display osteopetrosis. This is the first study providing evidence that

Table 3 μCT imaging[a]

	Wild-type mice	CAII-deficient mice	% change	*p*
Cortical bone				
Volume (mm^3)	0.646 ± 0.053	0.368 ± 0.204	↓ 43.0	<0.005
Bone volume (BV/TV; %)	83.7 ± 1.6	79.2 ± 2.3	↓ 5.4	<0.01
Cortical thickness (mm)	0.319 ± 0.018	0.237 ± 0.014	↓ 25.7	<0.005
BS/BV (1/mm)	6.27 ± 0.35	8.46 ± 0.51	↑ 34.9	<0.005
BMD (g/mm^3)	1.49 ± 0.04	1.42 ± 0.04	↓ 4.7	<0.05
Trabecular bone				
Bone volume (BV/TV; %)	16.9 ± 1.8	22.2 ± 4.0	↑ 31.4	<0.005
Trabecular no. (1/mm)	3.97 ± 0.34	6.06 ± 0.56	↑ 52.6	<0.001
Trabecular thickness (mm)	0.043 ± 0.003	0.037 ± 0.004	↓ 14.0	<0.005
Trabecular spacing (mm)	0.211 ± 0.020	0.130 ± 0.018	↓ 38.4	<0.001
BS/BV (1/mm)	47.2 ± 3.6	54.7 ± 5.0	↑ 15.9	<0.005
BMD (g/mm^3)	0.74 ± 0.03	0.66 ± 0.07	↓ 10.8	<0.05

Note. Cortical bone parameters were measured from the tibia-fibula junction. Trabecular bone parameters were measured from the tibial plateau

[a] Data expressed as mean ± standard deviation

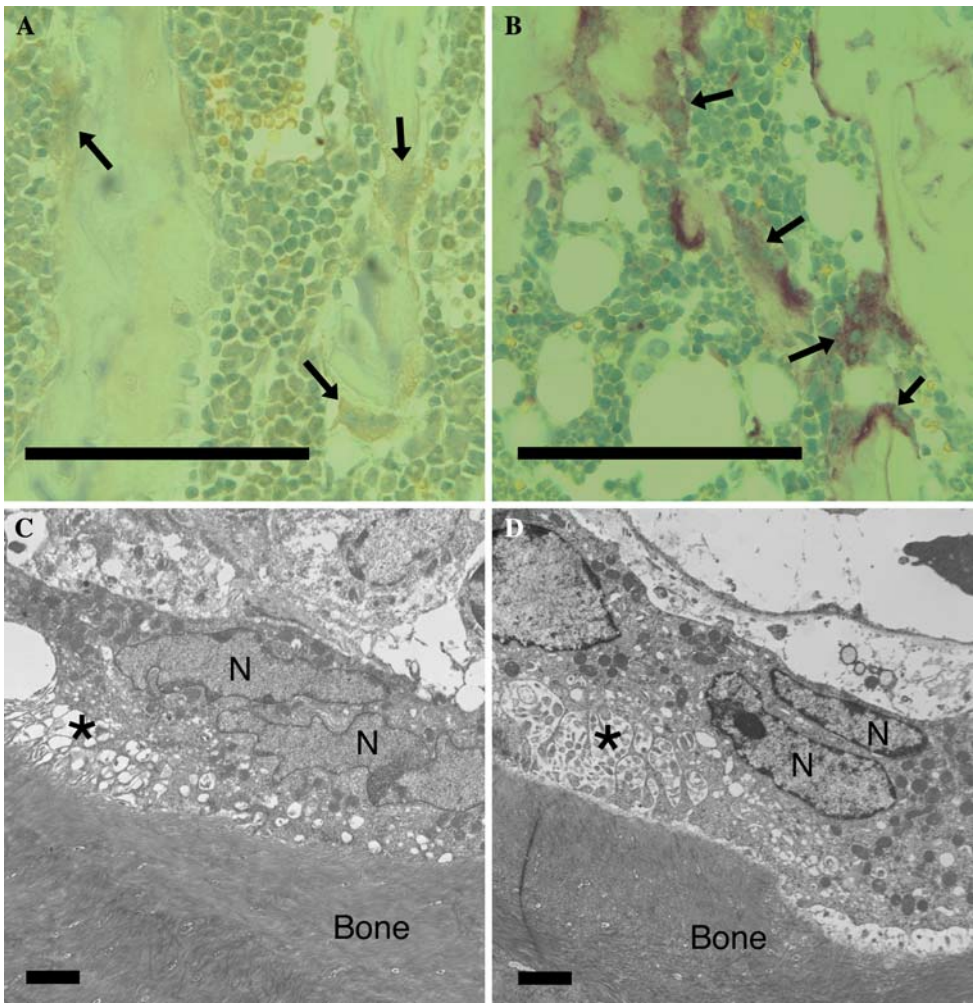

Fig. 3 Sagittal cross sections through the tibial plateau of WT (**A**) and CAII-deficient (**B**) mice showing that CAII-deficient mice have increased numbers of osteoclasts (arrows). The osteoclasts of WT (**C**) and CAII-deficient (**D**) mice visualized using transmission electron microscopy demonstrated multiple nuclei (N) and ruffled borders (*). Scale bar = 100 μm (A, B) and 2 μm (C, D)

CAII-deficient mice display phenotypic changes consistent with osteopetrosis in trabecular bone.

In previous studies, qualitative descriptions of the bones in CAII mice had indicated no structural changes aside from the decreased size of the bones and attribute the smaller bones to the smaller size of the mice [5, 6]. The overall decreased mass and length of the tibiae of CAII-deficient mice noted in this study are consistent with these previous reports. The quantitative histological and μCT analysis demonstrated a small but statistically significant, 4–5%, decrease in the cortical bone volume of CAII-deficient mice (Tables 2 and 3). This relatively minor difference may explain why previous studies that have only looked at gross radiographic findings [5] or qualitative histological structure [6] have not noted any significant changes.

Grossly, the metaphyseal widening of the tibial plateau was seen because the measured width of the tibiae at this level was similar in CAII-deficient and WT mice despite the smaller size of the bones in CAII-deficient mice (Table 1). Both histological and μCT analysis demonstrated that CAII-deficient mice had an increased trabecular bone volume (Tables 2 and 3), which was a result of the increased trabecular number and decreased spacing. It is unlikely that the increased trabecular bone volume is due to increased osteoblast activity because the bone formation rate is decreased in CAII-deficient mice (Table 2). The high bone volume and low bone formation rate indicate that trabecular bone resorption is inhibited in CAII-deficient mice [12]. We conclude that changes in the trabecular bone structure due to deficient bone resorption are characteristic of osteopetrosis in CAII-deficient mice. The CAII-deficient mice appear to compensate for reduced osteoclast activity by increasing the osteoclcast number (Table 2).

The CAII-deficient mice used in this study have been backcrossed to C3H mice for more than five generations, while the original CAII strain was on a C57BL/6J CAR-2 background. The C3H mouse strain has a higher bone mineral density [15] and bone turnover [16] compared to the C57BL6 strain, and C3H mice are less sensitive to limb loading [17]. Although there is a possibility that backcrossing the CAII-deficient mouse to a different strain may have unmasked the phenotype of osteopetrosis in

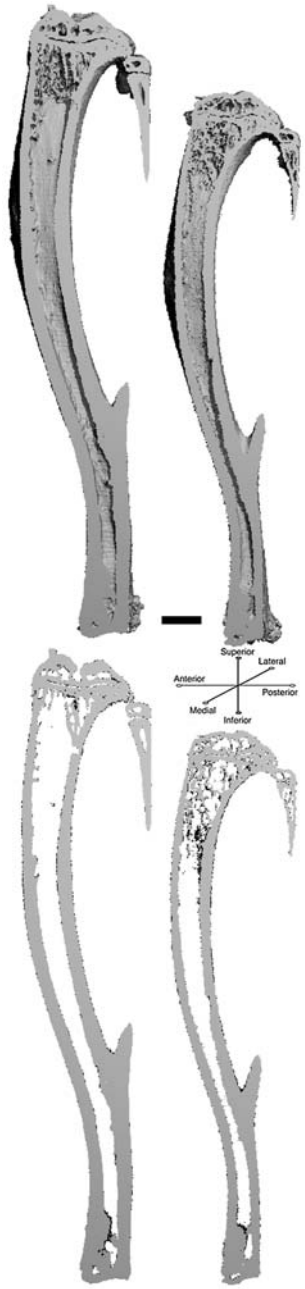

Fig. 4 A midsagittal section through the tibia of WT (left) and CAII-deficient (right) mice. The upper set of cross-sectional images displays a three-dimensional image of the bone, while the bottom section demonstrates an 18-μm-thick section at the same level. The cortical bone of CAII-deficient mice appears smaller than, but similar in bone volume to, that of WT mice, while the trabecular bone volume is significantly increased in CAII-deficient mice. Scale bar = 1 mm

trabecular bone described in this report, the CAII-deficient mice appeared qualitatively similar to those previously described [5, 6], and the phenotypic differences measured in this study were most apparent in quantitative histology, histomorphometry, and μCT analysis of trabecular bone, which had never been performed.

Although mutations that alter osteoclastogenesis are either intrinsic or extrinsic to the osteoclast, mutations affecting the function of osteoclasts are intrinsic [1]. Genetic mutations causing intrinsic defects in osteoclast acidification are responsible for more than 75% of pediatric patients with severe autosomal recessive osteopetrosis, emphasizing the importance of animal models of osteopetrosis with defects in the osteoclast acidification pathway [18–20]. In normal osteoclasts the resorption lacunae is acidified by protons generated in the cell cytoplasm from the action of CAII, an enzyme that catalyzes the equilibration of carbon dioxide and carbonic acid. The protons are transported to the resorption lacunae by an osteoclast specific H^+-ATPase that is coupled to a chloride channel that maintains charge neutrality. Autosomal recessive osteopetrosis arises from known mutations in TClRG1 (part of the osteoclast specific H^+-ATPase), ClCN7 (the gene encoding the chloride channel), and CAII [1].

Patients with defects in the osteoclast H^+-ATPase suffer from severe autosomal recessive osteopetrosis that is typically fatal within the first decade [1, 18]. There are more variable phenotypes among patients with chloride channel mutations, where both autosomal recessive and autosomal dominant mutations have been reported [20]. Patients with autosomal recessive osteopetrosis due to chloride channel defects account for a significant portion of patients with severe osteopetrosis, although some of these patients also have intermediate forms of the disease [1, 20, 21]. In contrast to patients with defects in the osteoclast H^+-ATPase or chloride channel, the osteopetrosis resulting from CAII deficiency is less severe [1, 22]. While the life expectancy of patients with CAII deficiency is unknown, patients with osteopetrosis due to CAII deficiency live longer than those with defects in the osteoclast H^+-ATPase or chloride channel [1, 22]. The skeletal disease in patients with CAII deficiency is variable; most do not suffer from fractures [22] and do not demonstrate hematologic failure, although many demonstrate signs of cranial nerve compression and variable mental retardation [1, 22]. Indeed, one report of a patient with CAII deficiency did not demonstrate radiographic changes sufficient to diagnose osteopetrosis [4]. Additionally, the bone disease caused by CAII deficiency is unique because the osteopetrosis has been noted to improve with age in untreated patients, whereas patients with other forms of osteopetrosis generally show progressively worse disease as they age [1, 22, 23]. It has been hypothesized that the osteopetrosis in CAII deficiency may begin to resolve due to renal tubular acidosis, which is also present in CAII-deficient patients, but not in patients with TClRG1 and ClCN7 mutations [1, 22].

The severe autosomal recessive forms of osteopetrosis arising from defects in the osteoclast H^+-ATPase or the chloride channel have mouse models with defects in

analogous genes. Both Atp6i knockout mice and oc/oc mice, which have a naturally occurring deletion in the Atp6i gene, develop an osteopetrotic phenotype with a decreased life span due to a defective osteoclast H^+-ATPase [24–26]. Additionally, ClCN7 knockout mice develop osteopetrosis and die within 6–7 weeks [27]. The severity of osteopetrosis in these animals may lead to decreased life span because of reduced hematopoiesis. Atp6i knockout mice have abnormal marrow cavities [24]. In ClCN7 knockout mice, no marrow space is evident on gross and microscopic examination [25], which leads to splenomegaly and anemia [27]. In contrast, CAII-deficient mice, although small in size, have a similar life span and bone marrow cavity compared to WT mice.

Another difference between the CAII-deficient mice is the normal appearance of cortical and trabecular bone. CAII-deficient mice have proportionally smaller cortical bones with a normal appearance, while the cortical bone is thin and morphologically disrupted in Atp6i and ClCN7 knockout mice [24, 27]. The trabecular bone volume has not been measured in Atp6i knockout mice (it is visibly increased), and has been shown to increase by 700% in 42-day-old ClCN7 [24, 27], but was only increased by 50% in CAII-deficient mice.

The differences in bone structure between these mouse models may result from differences in the function of osteoblasts and osteoclasts. In ClCN7 deficient mice, calcein labeling did not show an increase in bone apposition [27], while calcein labeling in CAII-deficient mice showed decreased bone formation. Although no quantitative values for osteoclast number have been reported, ClCN7 knockout mice have numerous small osteoclasts that attach to bone but do not form well-developed ruffled borders or show resorption lacunae [25, 27]. Quantitative and morphological differences have not been shown in the osteoclasts of Atp6i-deficient animals, but similarly to ClCN7 mice, the osteoclasts attach to bone but do not show any signs of resorption [24]. The presence of osteoclasts in CAII-deficient mice confirms that these mice do not show defects in osteoclast differentiation, similar to other mice with defects in osteoclast acidifcation. Similarly to ClCN7 and Atp6i knockout mice, the osteoclasts in CAII-deficient mice are increased in number, but unlike ClCN7 and Atp6i knockout mice, they show evidence of activity, as some osteoclasts formed resorption lacunae that contained scalloped edges.

In addition to skeletal manifestations of these defects, renal function has also been studied in Atp6i knockout mice. Similar to what is seen clinically, the Atp6i knockout mice do not demonstrate impaired renal function and have normal blood and urine pH [24]. One reason CAII-deficient mice may be able to maintain some function without necessitating CAII to generate protons is that the mice have a substantially lower arterial blood pH (7.18–7.25) due to a mixed metabolic and respiratory acidosis [7, 28], and the low extracellular pH has a stimulatory effect on osteoclasts [29–32]. While cell culture experiments have shown that decreasing the expression of CAII in osteoclasts using antisense nucleotides results in an inability of osteoclasts to resorb bone [33], another experiment showed that in the presence of a low extracellular pH, inhibiting CAII did not inhibit bone resorption in mature osteoclasts as it did when the extracellular pH was 7.4 [34]. This demonstrates that a low extracellular pH can compensate for acetazolamide-inhibited CAII function [34]. This experiment further showed that inhibiting CAII function inhibited osteoclast precursor proliferation and fusion [34]. For this reason it was unknown whether the primary defect in CAII deficiency results from reduced osteoclast number, decreased osteoclast function, or a combination of both. Our study shows that CAII-deficient mice had increased numbers of osteoclasts and a normal appearance of osteoclasts with a ruffled border (Fig 3), indicating that inhibited resorption, rather than reduced osteoclast number, is the primary mechanism in vivo. Furthermore, chronic acidosis has been shown to upregulate the H^+-ATPase in osteoclast cell cultures [35], which enhances the osteoclasts' ability to concentrate protons in the resorption lacunae. While this effect has not been demonstrated in vivo, it is possible that the CAII-deficient osteoclast may also maintain function by upregulation of the H^+-ATPase in the presence of chronic acidosis.

One unexpected finding in this study, which may be consistent with acidosis, was that both the cortical and the trabecular bone in CAII-deficient mice have a lower bone mineral density than WT mice (Table 3). This result appears to agree with previously published planar x-ray evidence of an aged CAII-deficient mouse [5], but the decreased radiopacity noted in the planar x-ray could have been due to size differences in the bone. Bone mineral density measured with μCT is directly related to the image intensity, as each cross-sectional image is the same thickness. Lower bone mineral density is consistent with acidosis, and not osteopetrosis, as both in vivo [36, 37] and in vitro studies [29] have demonstrated that acid loads stimulate physiochemical dissolution of mineralized bone matrix. Mineral dissolution occurs prior to organic matrix degradation. The lower bone mineral density found in CAII mice may facilitate osteoclast activity by promoting bone resorption or inhibiting complete matrix mineralization, mitigating the severity of osteopetrosis.

The CAII-deficient mouse demonstrated lower bone formation at all the measured locations. Decreased bone formation could be a result of osteoclast dysfunction, as osteoblast development and function are directly coupled to osteoclasts, or due to systemic factors, since osteoblasts are also sensitive to hormonal changes and alterations in

extracellular pH. In cortical bone, osteoclast-mediated bone formation (at the endosteal surface) was inhibited to a greater extent than osteoclast-independent bone formation (at the periosteal surface), demonstrating that inhibited osteoclast function may be partially responsible for the decreased bone formation. The acidosis in CAII-deficient mice would also be expected to decrease the bone formation rate, as osteoblast function is inhibited in chronic acidosis [38, 39]. This is particularly true in metabolic acidosis [32]. The decreased bone formation rate may be a feature of CAII-deficient mice that is not present in patients, as measurements of bone formation in CAII deficient patients have generally shown normal to increased activity [22]. The mechanism for this discrepancy is unclear, since CAII-deficient mice, like most patients with CAII deficiency, have mutations resulting in loss of CAII function [40, 41] and the arterial blood pH is similar between CAII-deficient mice and patients [3, 4].

In conclusion, the CAII-deficient mouse demonstrates some skeletal characteristics consistent with mild osteopetrosis. Although mice are less severely affected by skeletal abnormalities than most patients with a CAII deficiency, CAII-deficient mice demonstrate metaphyseal widening of the tibial plateau and increased trabecular bone volume, indicating the potential for use of CAII-deficient mice to study osteopetrosis. Understanding why the mice are generally less affected than patients and why trabecular bone seems to be preferentially affected in CAII-deficient mice will provide insight into the development of osteopetrosis caused by defects in osteoclast acidification and may implicate therapeutic targets for patients with CAII deficiency. Overall, the CAII-deficient mouse provides a valuable animal model for understanding the relationship between blood pH and both osteoblast and osteoclast function in osteopetrosis. When using this model the differences in presentation between mice and patients outlined in this study should be kept in mind.

Acknowledgments This work was supported by a grant from the Dialysis Clinic, Inc., a not-for-profit organization and by Grants NIHT35 HL07479 and NBIB P41-EB002035-5. D. S. Margolis was supported in part by the NIH through Graduate Training in Physiology Grant HL07249 and Short-Term Training: Students in Health Professional Sciences Grant T35HL07479, and J.A. Szivek was supported in part by NIBIB Grant R01-EB00060. The histological data were generated by the TACMASS (Tissue Acquisition and Cellular/Molecular Analysis Shared Service) Core at the Arizona Cancer Center, supported by NIH Grant CA23074. The TEM data were generated by the Arizona Research Labs Division of Biotechnology CORE imaging facility.

References

1. Tolar J, Teitelbaum SL, Orchard PJ (2004) Mechanisms of disease: osteopetrosis. N Engl J Med 351:2839–2849
2. Sly WS, Whyte MP, Hewettemmett D, Yu YSL, Tashian RE (1983) Carbonic anhydrase-II deficiency identified as the primary defect in four kindreds with the syndrome of osteopetrosis–renal tubular-acidosis–basal ganglia calcification. Calcif Tissue Int 35:688–688
3. Ohlsson A, Stark G, Sakati N (1980) Marble brain disease – recessive osteopetrosis, renal tubular-acidosis and cerebral calcification in 3 Saudi Arabian fFamilies. Dev Med Child Neurol 22:72–84
4. Ohlsson A, Cumming WA, Paul A, Sly WS (1986) Carbonic anhydrase-II deficiency syndrome –recessive osteopetrosis with renal tubular-acidosis and cerebral calcification. Clin Invest Med 9:A139–A139
5. Lewis SE, Erickson RP, Barnett LB, Venta PJ, Tashian RE (1988) N-Ethyl-N-nitrosourea induced null mutation at the mouse car-2 locus—an animal-model for human carbonic anhydrase-II deficiency syndrome. Proc Natl Acad Sci USA 85:1962–1966
6. Jepsen KJ, Goldstein SA, Biesecker LG, Spicer SS, Erickson RP (1990) The mechanical properties of cortical bone from carbonic anhydrase II deficient mice. Am J Hum Genet 47S:A159
7. Lien YHH, Lai LW (1998) Respiratory acidosis in carbonic anhydrase II-deficient mice. Am J Physiol 274:L301–L304
8. Lai LW, Chan DM, Erickson RP, Hsu SJ, Lien YHH (1998) Correction of renal tubular acidosis in carbonic anhydrase II-deficient mice with gene therapy. J Clin Invest 101:1320–1325
9. Tashian RE (1992) Genetics of the mammalian carbonic-anhydrases. Adv Genet 30:321–356
10. Emmanual J, Hornbeck C, Bloebaum RD (1987) A poly(methyl methacrylate method for large specimens of mineralized bone with implants. Stain Technol 62:401–410
11. Villanueva AR, Lundin KD (1989) A versatile new mineralized bone stain for simultaneous assessment of tetracycline and osteoid seams. Stain Technol 64:129–138
12. Parfitt AM, Drezner MK, Glorieux FH, Kanis JA, Malluche H, Meunier PJ, Ott SM, Recker RR (1987) Bone histomorphometry—standardization of nomenclature, symbols, and units. J Bone Miner Res 2:595–610
13. Spurr AR (1969) A low-viscosity epoxy resin embedding medium for electron microscopy. J Ultrastruct Res 26:31
14. Margolis DS, Kim D, Szivek JA, Lai LW, Lien YH (2006) Functionally improved bone in calbindin-D28k knockout mice. Bone 39:477–484
15. Beamer WG, Donahue LR, Rosen CJ, Baylink DJ (1996) Genetic variability in adult bone density among inbred strains of mice. Bone 18:397–403
16. Sheng MHC, Baylink DJ, Beamer WG, Donahue LR, Rosen CJ, Lau KHW, Wergedal JE (1999) Histomorphometric studies show that bone formation and bone mineral apposition rates are greater in C3H/HeJ (high-density) than C57BL/6J (low-density) mice during growth. Bone 25:421–429
17. Kodama Y, Umemura Y, Nagasawa S, Beamer WG, Donahue LR, Rosen CR, Baylink DJ, Farley JR (2000) Exercise and mechanical loading increase periosteal bone formation and whole bone strength in C57BL/6J mice but not in C3H/Hej mice. Calcif Tissue Int 66:298–306
18. Frattini A, Orchard PJ, Sobacchi C, Giliani S, Abinun M, Mattsson JP, Keeling DJ, Andersson AK, Wallbrandt P, Zecca L, Notarangelo LD, Vezzoni P, Villa A (2000) Defects in TCIRG1 subunit of the vacuolar proton pump are responsible for a subset of human autosomal recessive osteopetrosis. Nat Genet 25: 343–346
19. Sobacchi C, Frattini A, Orchard P, Porras O, Tezcan I, Andolina M, Babul-Hirji R, Baric I, Canham N, Chitayat D, Dupuis-Girod S, Ellis I, Etzioni A, Fasth A, Fisher A, Gerritsen B, Gulino V, Horwitz E, Klamroth V, Lanino E, Mirolo M, Musio A, Matthijs G, Nonomaya S, Notarangelo LD, Ochs HD, Furga AS, Valiaho

J, van Hove JLK, Vihinen M, Vujic D, Vezzoni P, Villa A (2001) The mutational spectrum of human malignant autosomal recessive osteopetrosis. Hum Mol Genet 10:1767–1773
20. Frattini A, Pangrazio A, Susani L, Sobacchi C, Mirolo M, Abinun M, Andolina M, Flanagan A, Horwitz EM, Mihci E, Notarangelo LD, Ramenghi U, Teti A, Van Hove J, Vujic D, Young T, Albertini A, Orchard PJ, Vezzoni P, Villa A (2003) Chloride channel ClCN7 mutations are responsible for severe recessive, dominant, and intermediate osteopetrosis. J Bone Miner Res 18:1740–1747
21. Cleiren E, Benichou O, Hul EV, Gram J, Bollerslev J, Singer FR, Beaverson K, Aledo A, Whyte MP, Yoneyama T, deVernejoul MC, Hul WV (2001) Albers-Schonberg disease (autosomal dominant osteopetrosis, type II) results from mutations in the CICN7chloride channel gene. Hum Mol Genet 10:2861–2867
22. Whyte MP (1993) Carbonic anhydrase-II deficiency. Clin Orthop Relat Res 294:52–63
23. Whyte MP, Murphy WA, Fallon MD, Sly WS, Teitelbaum SL, McAlister WH, Avioli LV (1980) Osteopetrosis, renal tubular-acidosis and basal ganglia calcification in three sisters. Am J Med 69:64–74
24. Li YP, Chen W, Liang YQ, Li E, Stashenko P (1999) Atp6i-deficient mice exhibit severe osteopetrosis due to loss of osteoclast-mediated extracellular acidification. Nat Genet 23:447–451
25. Marks SC, Seifert MF, Lane PW (1985) Osteosclerosis, a recessive skeletal mutation on chromosome 19 in the mouse. J Hered 76:171–176
26. Scimeca JC, Franchi A, Trojani C, Parrinello H, Grosgeorge J, Robert C, Jaillon O, Poirier C, Gaudray P, Carle GF (2000) The gene encoding the mouse homologue of the human osteoclast-specific 116-kDa V-ATPase subunit bears a deletion in osteosclerotic (oc/oc) mutants. Bone 26:207–213
27. Kornak U, Kasper D, Bosl MR, Kaiser E, Schweizer M, Schulz A, Friedrich W, Delling G, Jentsch TJ (2001) Loss of the CIC-7 chloride channel leads to osteopetrosis in mice and man. Cell 104:205–215
28. Brion LP, Cammer W, Satlin LM, Suarez C, Zavilowitz BJ, Schuster VL (1997) Expression of carbonic anhydrase IV in carbonic anhydrase II-deficient mice. Am J Physiol 42:F234–F245
29. Bushinsky DA, Frick KK (2000) The effects of acid on bone. Curr Opin Nephrol Hypertens 9:369–379
30. Meghji S, Morrison MS, Henderson B, Arnett TR (2001) pH dependence of bone resorption: mouse calvarial osteoclasts are activated by acidosis. Am J Physiol 280:E112–E119
31. Bushinsky DA (1996) Metabolic alkalosis decreases bone calcium efflux by suppressing osteoclasts and stimulating osteoblasts. Am J Physiol 40:F216–F222
32. Bushinsky DA (1995) Stimulated osteoclastic and suppressed osteoblastic activity in metabolic but not respiratory-acidosis. Am J Physiol 37:C80–C88
33. Laitala T, Vaananen HK (1994) Inhibition of bone-resorption in-vitro by antisense RNA and DNA-molecules targeted against carbonic-anhydrase-II or 2 subunits of vacuolar H+-ATPase. J Clin Invest 93:2311–2318
34. Lehenkari P, Hentunen TA, Laitala-Leinonen T, Tuukkanen J, Vaananen HK (1998) Carbonic anhydrase II plays a major role in osteoclast differentiation and bone resorption by effecting the steady state intracellular pH and Ca^{2+}. Exp Cell Res 242:128–137
35. Nordstrom T, Shrode LD, Rotstein OD, Romanek R, Goto T, Heersche JNM, Manolson MF, Brisseau GF, Grinstein S (1997) Chronic extracellular acidosis induces plasmalemmal vacuolar type H^+ ATPase activity in osteoclasts. J Biol Chem 272:6354–6360
36. Lemann J, Litzow JR, Lennon EJ (1966) Effects of chronic acid loads in normal man—further evidence for participation of bone mineral in defense against chronic metabolic acidosis. J Clin Invest 45:1608–1614
37. Phelps KR, Einhorn TA, Vigorita VJ, Lieberman RL, Uribarri J (1986) Acidosis-induced osteomalacia—metabolic studies and skeletal histomorphometry. Bone 7:171–179
38. Frick KK, Bushinsky DA (1999) In vitro metabolic and respiratory acidosis selectively inhibit osteoblastic matrix gene expression. Am J Physiol 277:F750–F755
39. Frick KK, Bushinsky DA (1998) Chronic metabolic acidosis reversibly inhibits extracellular matrix gene expression in mouse osteoblasts. Am J Physiol 44:F840–F847
40. Hu PY, Lim EJ, Ciccolella J, Strisciuglio P, Sly WS (1997) Seven novel mutations in carbonic anhydrase II deficiency syndrome identified by SSCP and direct sequencing analysis. Hum Mutat 9:576–576
41. Shah GN, Bonapace G, Hu PY (2004) Carbonic anhydrase II deficiency syndrome (osteopetrosis with renal tubular acidosis and brain calcification): novel mutations in CA2 identified by direct sequencing expand the opportunity for genotype-phenotype correlation. Hum Mutat 24:272